Complex flow patterns at the onset of annular electroconvection in a dielectric liquid subjected to an arbitrary unipolar injection

Jian Wu and **Alberto T. Pérez**
Departamento de Electrónica y Electromagnetismo, Universidad de Sevilla
Facultad de Física, Avenida Reina Mercedes s/n
41012 Sevilla, Spain

and **Philippe Traoré**
Institut PPRIME, Département Fluide-Thermique-Combustion
Boulevard Pierre et Marie Curie, BP 30179
86962 Futuroscope-Chasseneuil, France

and **Pedro A. Vázquez**
Departamento de Física Aplicada III, Universidad de Sevilla
ESI, Camino de los Descubrimientos s/n
41092 Sevilla, Spain

ABSTRACT

We numerically investigated the annular electroconvection that takes place in a dielectric liquid lying between two concentric cylinder electrodes. A uniform injection of arbitrary strengths either from the inner or outer cylinder introduces free charge carriers into the system, and the resulting Coulomb force induces electroconvection. The problem is characterized by a linear instability that corresponds to the onset of flow motion. The linear stability criteria were determined from direct numerical results and by linear stability analysis, and the results obtained with the two approaches show an excellent agreement. We focused on the fully developed flow pattern in the finite amplitude regime. We observed very different flow motions that were highly dependent on the injection strength.

Index Terms — **Electrohydrodynamics; dielectric liquid; charge injection; numerical analysis; annular geometry.**

1 INTRODUCTION

ELECTRO-hydrodynamics (EHD) deals with the interaction between the electric field and the fluid motion [1]. A fundamental problem in EHD is concerned with the Coulomb-driven convection in a single-phase dielectric liquid [2,3]. The Coulomb force exerting on the free space charges serves as a body force and drives the flow motion. The induced motion contributes to the passage of electric current, and the consequent voltage-current characteristics. There are two main sources for free space charges in an isothermal liquid: the charge injection at the electrode/liquid interface [4,5] and the field-enhanced dissociation in the bulk liquid [6,7]. For a liquid of low conductivity and subjected to a high electric field, the charge injection mechanism often plays the dominant role in generating space charges [2,3,8].

In this study we consider the limit case that ions are injected from one electrode (i.e. unipolar injection) into a perfectly insulating liquid. Various electrode shapes and configurations, symmetrical or asymmetrical, have been considered to study EHD flows [9]. The symmetrical configurations (e.g., the parallel plates, concentric cylinders and spheres) are particularly interesting due to that under some assumptions the system may possess a linear instability bifurcation. This means that the driving Coulomb force is required to be sufficiently strong to overcome the viscous damping, and then the flow motion will arise. The prediction and understanding of the onset flow motion can be viewed as a first and also critical step in understanding more complex phenomena.

Previous studies mainly focused on the simplest parallel plate configuration, whereas less attention was paid to the configurations of cylinder and sphere. It is interesting to point out that the electroconvection between two parallel plates shares strong analogy with the classic Rayleigh-Bénard convection (RBC) that happens in a planar liquid layer heated from below [3]. However, such analogy no longer exists for the cylindrical geometry that we will consider in this study.

Instead, we may compare the annular electroconvection to the Taylor-Couette (TC) flow in the gap between two rotating cylinders [10]. The change of the configuration from plate to cylinder complicates the problem by introducing two new factors: the injection direction (from the inner or outer cylinder) and the radius ratio between the two electrodes. From the practical application point of view, the cylinder configuration is more interesting than the plate one. A typical example is concerned with the heat transfer enhancement in tubes (wire/cylinder) [11].

The linear stability analysis with the unipolar injection induced annular electroconvection in a dielectric liquid lying between two concentric cylinder electrodes was performed two or three decades ago in a series of studies [12,13,14]. Very recently, Fernandes et al. revisited the problem and conducted a 2D normal-mode linear stability analysis [15]. In addition, they also performed the first direct numerical simulation with this configuration [16]. Only the strong injection case of C=10 (C being the dimensionless injection strength parameter) was considered in their numerical study. For this injection strength, they observed a stationary flow pattern in the finite amplitude regime, which means the driving parameter is slightly higher than the linear stability criterion, no matter which direction the charges are injected and the radius ratio. Furthermore, they also extended the driving parameter far away from the linear stability criteria, and they observed oscillatory and chaotic flows.

One core difficulty in simulating Coulomb-driven convection lies in the method for the charge conservation equation, which is strongly convection-dominated. In [17], we borrowed the so-named total variation diminishing (TVD) schemes from the field of computational gas dynamics, and applied them to the charge conservation equation. We investigated the electroconvection in the plate configuration induced by strong and weak injection in [17] and [18], respectively. We noticed the very different flow patterns at the onset of motion in the weak and strong injection regimes. In our recent study [19], we developed an efficient method for the electric field–space charge coupled problems with complex geometries. Later in [20], we coupled the method of [19] with a Navier-Stokes solver, and with the new tool we studied the annular electroconvection induced by a strong unipolar injection. For direct comparsion to the results in [16,17], the injection strength C in [20] is also fixed to 10. In [20] we focused on the flow's subcritical bifurcation behavior, a very characteristic feature of Coulomb-driven convection. In addition, a complete bifurcation diagram in the finite amplitude regime was also provided in that study.

We extend here the study to arbitrary injection strength. The first numerical results of annular electroconvection in weak and medium injection regimes will be presented. The linear stability criteria predicted by the stability analysis will be used to verify our direct numerical results in the first place. Then we will highlight the complex flow patterns relating to the injection strength in the finite amplitude regime. The remainder of the paper is organized as follows. In Section 2, we present the physical problem, governing equations and boundary conditions. In Section 3, the methods are briefly described. Results and discussion are presented in Section 4. Finally, in Section 5, we summarize our findings and suggest some working directions.

2 PROBLEM FORMULATION

This section covers the description of the physical problem, the governing equations, the dimensionless parameters, and the boundary conditions.

2.1 PHYSICAL PROBLEM

We consider a layer of perfectly insulating liquid lying between two concentric infinite cylinder electrodes and subjected to an electrical potential difference ΔV. The physical problem is sketched in Figure 1, along with the Cartesian coordinate system used in this work. The two-dimensional problem is considered. The applied voltage produces a radial electric field and charge injection from the emitter electrode into the bulk. The injection is from only one electrode, either from the inner or the outer side. The injection is assumed to be *homogeneous* and *autonomous*, which means the injected charge density always takes a constant value, neither influenced by the local electric field nor the flow motion [2, 3]. The radii of the inner and outer cylinders are R_i and R_o, respectively. The fluid of density ρ, dynamic viscosity η and permittivity ε, is assumed to be incompressible and Newtonian.

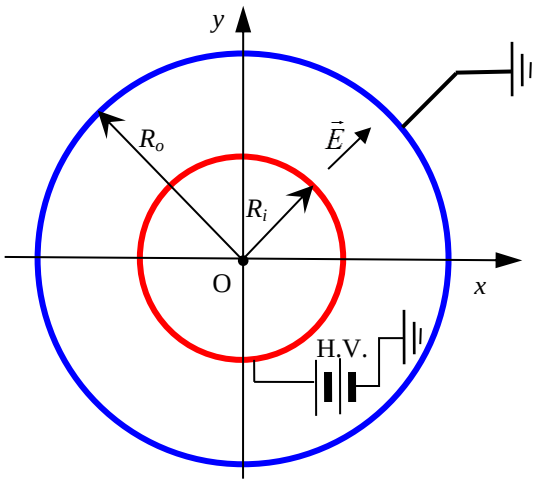

Figure 1. Sketch of annular electroconvection between two cylinders.

The physical problem owns complex and strong nonlinear couplings. First, the appearance of space charges modifies the electric field, which in turn affects the charge distribution via the ion drift mechanism. In addition, the flow is driven by the Coulomb force (i.e. the charge density distribution and electric field), while the distribution of space charges relies heavily on the fluid velocity field via the ion convection mechanism.

2.2 GOVERNING EQUATIONS

For an isothermal dielectric liquid under the effect of an electric field, the complete governing equations include a reduced set of Maxwell's equations in the electroquasistatics limit, and the Navier-Stokes equations [1]. Taking as scales H=(R_o-R_i) for length, ΔV for electric potential, $K\Delta V/H$ for

velocity, $\rho K^2\Delta V^2/H^2$ for pressure, $H^2/K\Delta V$ for time and $\varepsilon\Delta V/H^2$ for charge density, the resulting non-dimensional governing equations are [1,8,20]:

$$\nabla\cdot\vec{u}=0\,, \tag{1}$$

$$\frac{\partial\vec{u}}{\partial t}+(\vec{u}\cdot\nabla)\vec{u}=-\nabla\tilde{p}+\frac{M^2}{T}\Delta\vec{u}+M^2 q\vec{E}\ , \tag{2}$$

$$\frac{\partial q}{\partial t}+\nabla\cdot\left(q(\vec{u}+\vec{E})\right)=0\,, \tag{3}$$

$$\nabla^2 V=-q\,, \tag{4}$$

$$\vec{E}=-\nabla V\,, \tag{5}$$

where the vectors $\vec{u}\equiv[u,v]$ and $\vec{E}\equiv[E_x,E_y]$ denote the fluid velocity and electric field. The scalars V and q represent the electric potential and the space charge density. The modified pressure $\tilde{p}$ includes an extra contribution from the electrostriction force term [3]. The last term in (2) represents the Coulomb force. The diffusion term in the charge conservation equation (3) has been neglected to keep consistence with previous studies. Two dimensionless numbers appear in the above equations,

$$T=\frac{\varepsilon\Delta V}{\rho\nu K}\quad\text{and}\quad M=\frac{1}{K}\left(\frac{\varepsilon}{\rho}\right)^{1/2}.$$

The electric Rayleigh number T represents the ratio between the Coulomb force to the viscous force. The mobility number M is defined as the ratio between the so-called hydrodynamic mobility $(\varepsilon/\rho)^{1/2}$ to the true ionic mobility K. The definition equation shows that M depends only on the fluid properties.

Besides T and M, the problem also depends on the injection strength C, injection direction, and the radius ratio Γ. In dimensionless form, C and Γ are defined as

$$C=\frac{q_0 H^2}{\varepsilon\Delta V}\quad\text{and}\quad \Gamma=\frac{R_i}{R_o},$$

where q_0 is the injected charge density at emitter electrode.

According to [21], the injection strength can be preliminarily classified into three regimes: strong ($5<C$), medium ($0.2<C<5$), and weak ($C<0.2$). Different injection regimes can be experimentally achieved by different methods. Lacroix et al., [22] and Malraison and Atten [23] covered the electrodes with ion exchange membranes and obtained a Space-Charge-Limited (SCL, $C\to\infty$) injection; Denat et al., [24] and Mccluskey et al., [25] used bare electrodes and the liquids saturated with salts to produce a weak or medium injection; Zhang [26] also used bare electrodes and a liquid with no salt, and the injection was estimated to be weak.

2.3 BOUNDARY AND INITIAL CONDITIONS

The dimensionless domain is defined as the gap between the two cylinders, i.e. $\Gamma/(1-\Gamma)=R_i\le r\le R_o=1/(1-\Gamma)$, $0<\Gamma<1$ and $0\le\theta\le 2\pi$. The no-slip condition for velocity ($u=v=0$) is applied on the two cylinders. The constant electric potentials lead to $V=1$ and $V=0$ at the emitter and collector respectively. Since (3) is a hyperbolic equation, only one-side boundary condition is required for q. The assumption of *homogeneous* and *autonomous* injection leads to $q=C$ at the emitter.

Table 1. The Values for Coefficients A_e and B_e in Equation (6), $\Gamma=0.5$

C	Inner		Outer	
	A_e	B_e	A_e	B_e
0.05	0.266	27.281	0.264	-31.963
0.1	0.372	12.860	0.368	-17.542
0.5	0.772	1.382	0.729	-6.128
1.0	1.000	0.000	0.901	-4.811
5.0	1.390	-0.923	1.091	-4.048
10.0	1.439	-0.979	1.104	-4.012
20.0	1.455	-0.995	1.108	-4.003

The set of governing equations (1-5) together with the above boundary conditions possesses a hydrostatic solution, which means the fluid keeps rest while charges transfer solely by drift due to electric field. The hydrostatic solution may be expressed as [14]:

$$q_s=A_e\left[\delta\left(r^2+B_e\right)\right]^{-1/2}\ \text{and}\ E_s=\left(\frac{\delta A_e}{r}\right)\left[\delta\left(r^2+B_e\right)\right]^{1/2} \tag{6}$$

where δ = +1 and -1 for the inner and outer injection, respectively. The parameters A_e and B_e are two constants depending on C, Γ and the injection direction. The implicit functions used to determine A_e and B_e can be found in [14]. For some cases considered in this study, the values of A_e and B_e can be found in Table 1. The hydrostatic solutions serve as the initial conditions for direct numerical simulations.

3 METHODS

Several methods including the linear stability analysis, direct numerical simulation and a simple phenomenological modal analysis were employed in this study. The linear stability analysis method developed by Agrait and Castellanos [14] was adapted to study the 2D case with longitudinal modes. The critical stability criteria obtained by the linear stability analysis is used to verify direct numerical results. The modal analysis is used to understand the evolution of different modes, and the method was detailed in [20].

We developed an in-house direct numerical program based on a 2nd order finite volume method to solve equations (1-5) [27]. The solution domain is discretized with structured grids made up of nonorthogonal quadrilaterals. The collocated arrangement is employed, which means all variables are stored at the center of each quadrilateral mesh. The solver contains two modules: one for the Navier-Stokes equations (1-2) and the other one for the electrostatic equations (3-5). The two modules are coupled in a sequential procedure. For the Navier-Stokes equations, the central differencing (CD) scheme and the improved deferred correction (IDC) scheme [28] are used to compute the convective and diffusive fluxes, respectively. The 2nd order semi-implicit three time levels (I3L) scheme [27] is used for time integration. The coupling between the fluid velocity and pressure is undertaken by the SIMPLE algorithm [29]. To prevent the unphysical checker-

boarder pressure field with the collocated arrangement, the Rhie-Chow momentum interpolation [30] is implemented. The algorithm for electrostatic equations (3-5) is well explained in [19]. The Smooth Monotonic Algorithm for Real Transport (SMART) scheme [31] is applied to the charge conservation equation (3). An improved least-squares method [32] is used to calculate the electric field and other gradients. For more numerical details, please refer to [19, 33].

4 RESULTS AND DISCUSSION

The physical problem is fully defined by four dimensionless numbers (T, M, C and Γ) and the injection direction. In this study, we consider a representative radius ratio Γ=0.5 (i.e. R_i=1.0, R_o=2.0). The mobility number M is fixed as 60, which corresponds to the silicon oil used in the experimental studies of [25, 34]. The injection of arbitrary strength, either from the inner or outer cylinder, will be considered.

4.1 HYDROSTATIC SOLUTIONS AND GRID CONSIDERATION

We first validate our numerical solver by computing the hydrostatic solutions. In Figure 2 we have compared our numerical results of charge density distribution in the radial direction with the analytical ones. The numerical solutions are obtained by switching off the module for the Navier-Stokes equations. A perfect agreement is always obtained.

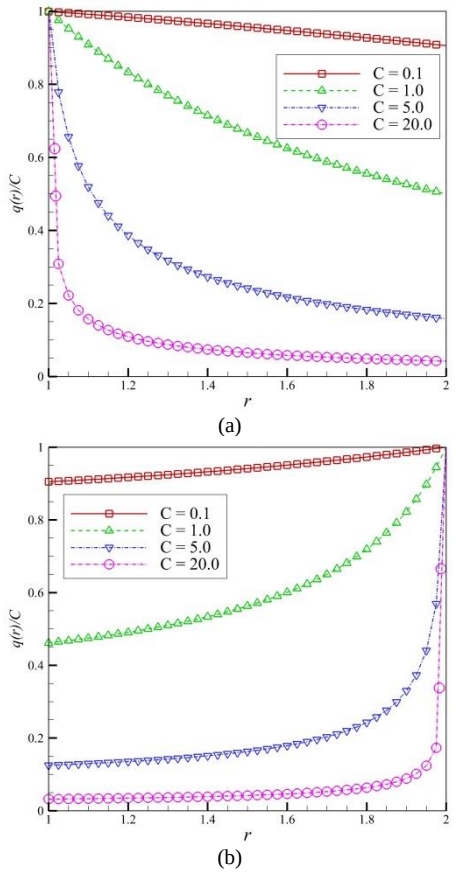

Figure 2. Comparison between the analytical and numerical charge density distributions at hydrostatic state: (a) inner injection, (b) outer injection. Note that the charge density q has been normalized with the injection strength C for better display.

For all injection strengths the charge density continually decreases from the emitter to the collector. In addition, along with the increase of C, the variation of charge density in the region close to the emitter becomes sharper. For the same injection strength, the outer injection case shows a more rapid decrease than the inner injection one. For example, for C=20 and the same small distance from the injector (say 0.05), the charge density drops 77.8% with inner injection while 87.6% with the outer case.

These distribution characteristics of charge density with the strength and direction of injection put forward different requirements for the grid design. A uniform grid works well for weak and medium injection, while a non-uniform (non-uniformity only appears in the radial direction) grid is very necessary for strong injection. After various grid convergence tests, we finally chose a uniform grid with 400×150 cells, a uniform grid with 450×150 cells, a non-uniform grid with 500×175 cells and a non-uniform grid with 500×200 cells for the computations of the weak injection (C<0.2, inner and outer), medium injection (0.2<C<5, inner and outer), inner strong injection (5<C), and outer strong injection (5<C), respectively.

4.2 LINEAR STABILITY CRITERIA

We have performed a stability analysis to analytically predict the linear stability criteria. The criteria are expressed through the critical electric Rayleigh number T_c and the critical Fourier mode m_c. The results are summarized in Figure 3. Note that the linear stability criteria are independent on the mobility number M.

For both injection directions, increasing C yields lower T_c, which implies that the system is more unstable in the strong regime than in the weak one, as a consequence of a greater Coulomb force for stronger injection. For very weak injection the value of T_c scales in such a way that T_cC^2 tends to a fixed value, the same behavior already observed in the configuration of parallel plates [35, 36]. Similarly, for $C>>1$, T_c tends towards a fixed value. This asymptotic behavior is due to that the presence of space charge limits the injected current and the Coulomb force in that limit.

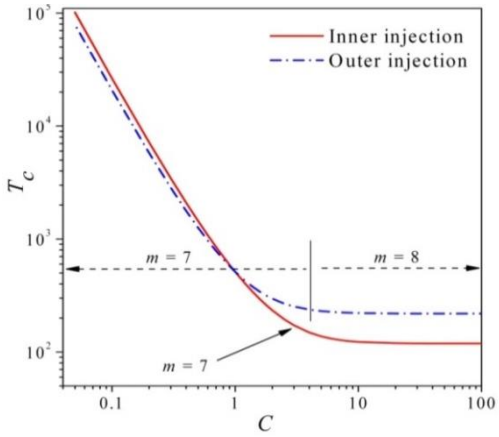

Figure 3. Variation of the critical electric Rayleigh number T_c and the critical Fourier mode m with the injection strength C.

Figure 3 shows that the outer injection configuration is more unstable than the inner injection one for weak injection

case. The inner injection case is the most unstable in the strong injection limit. The crossover takes place for $C \approx 1.0$. A similar behavior was found by Agra ï and Castellanos [14] including 3D modes and the 2D results of Fernandes et al. [16] with a different radius ratio. The differences between the critical values for weak injection are rather small, because, in this limit, the electric field is not affected by the injected charge. Things are different for the strong injection case, where a gradient of charge of geometrical origin superimposes to the gradient due to Coulomb repulsion, resulting in a more unstable situation.

Although the Fourier mode number, associated to the number of convective cells, remains unchanged for the inner injection configuration, it changes from 7 to 8 in the outer injection case.

4.3 DIRECT NUMERICAL RESULTS

To numerically determine the critical stability parameter, we gradually increase T from zero until we observe the onset of flow. Experimentally, this is done by increasing the applied voltage. For all cases (arbitrary strengths and both injection directions), we have found that the system keeps a rest state when $T<T_c$, and once T is just above T_c the system jumps to a convective state of a certain strength.

Table 2. Comparison Between Analytical and Numerical Predictions of the Linear Stability Criteria Expressed Through the Critical Electric Rayleigh Number T_c and the Critical Fourier mode m_c, I=0.5. Note That the Numerical Values of m_c are the Pair Numbers of Convective Cells at the Exponentially Growing Stage of Flow Motion.

C		Inner			outer		
		m_c	T_c	*Pattern*	m_c	T_c	*Pattern*
10.0	*A*	7	122.84	---	8	221.38	---
	N	7	122.75	*S*	8	220.71	*S*
5.0	*A*	7	137.62	---	8	230.43	---
	N	7	136.82	*S*	8	230.18	*S*
1.0	*A*	7	511.85	---	7	513.27	---
	N	7	510.96	*I*	7	512.94	*I*
0.5	*A*	7	1444.16	---	7	1258.53	---
	N	7	1448.01	*I*	7	1245.04	
0.1	*A*	7	26470.11	---	7	20827.23	---
	N	7	26441.80	*C*	7	20751.01	*C*
0.05	*A*	7	101603.92	---	7	79075.60	---
	N	7	100777.12	*C*	7	78944.30	*C*

*Note: the 2nd column: A-analytical, N-Numerical; the 5th and 8th column: S-stationary, I-*irregular, *C–chaotic*.

We have recorded the time histories of the maximum fluid velocity norm Vmax defined as $\mathrm{V}\max = \max\left[\sqrt{u^2+v^2}\right]$ and of the modal amplitudes. In addition, we have output the stream function and charge density distribution to show the flow structure. As we will present below in the Vmax – *time* figures, there are always three different stages for each case: an initial hydrostatic stage, the subsequent exponentially growing one, and the final stage corresponding to the fully developed convection. By checking the iso-contours of stream function at the second stage, there is a fixed number of counter-rotating vortex pairs that regularly distributed. The number of vortex pairs should be compared with the critical Fourier mode m_c predicted by the stability analysis [37]. We have extracted the growth rate of the second stage to numerically determine the critical electric Rayleigh number T_c [17, 38]. In Table 2 we have summarized some linear stability criteria determined from direct numerical results and analytically predicted by the stability analysis. A perfect agreement is shown for m_c, and the maximum discrepancy between the analytical and numerical values of T_c is less than 1%. The agreement between analytical and numerical stability criteria fully verified our numerical solver and stability analysis method.

However, the flow patterns at the third stage are diverse and highly dependent on the injection strength. We present below a detailed description of different flow patterns.

1) Stationary flow pattern

For $C \geq 2$ and both injection directions, a stationary flow pattern is finally formed. Figure 4 plots the time histories of Vmax for the representative case of C=5. The fluid velocity continuously increases from zero and reaches a maximum, and then remains constant. Figure 5 shows the charge density distribution and the corresponding stream function for the final steady convection.

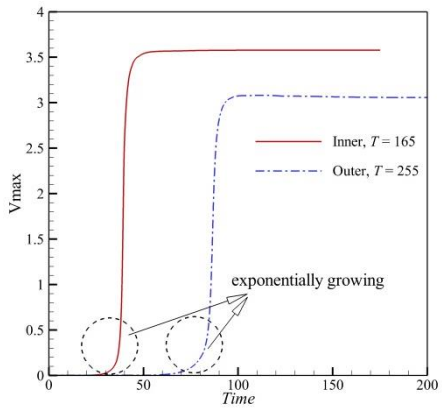

Figure 4. Time histories of the maximum velocity norm for strong injection regime, C=5. Note that the values of T_c for inner and outer injection are 137.62 and 230.43, respectively.

By checking the fluid velocity field and the electric field, we notice that the maximum fluid velocity in the radial direction (V_r = 3.672, inner; V_r = 3.315, outer) is higher than the maximum electric field (E_r = 1.300, inner; E_r = 1.890, outer), which means the charge density distribution is mainly controlled by the fluid motion. This results in a region strictly free of charges ($q \to 0$), a very characteristic feature of Coulomb-driven convection. There are 7 and 8 discrete charge void regions in Figures 5a and 5b, respectively. Each void region corresponds to a pair of counter-rotating convective cells; see Figures 5c and 5d. At beginning of the second stage, the positions of convective cells are chosen randomly.

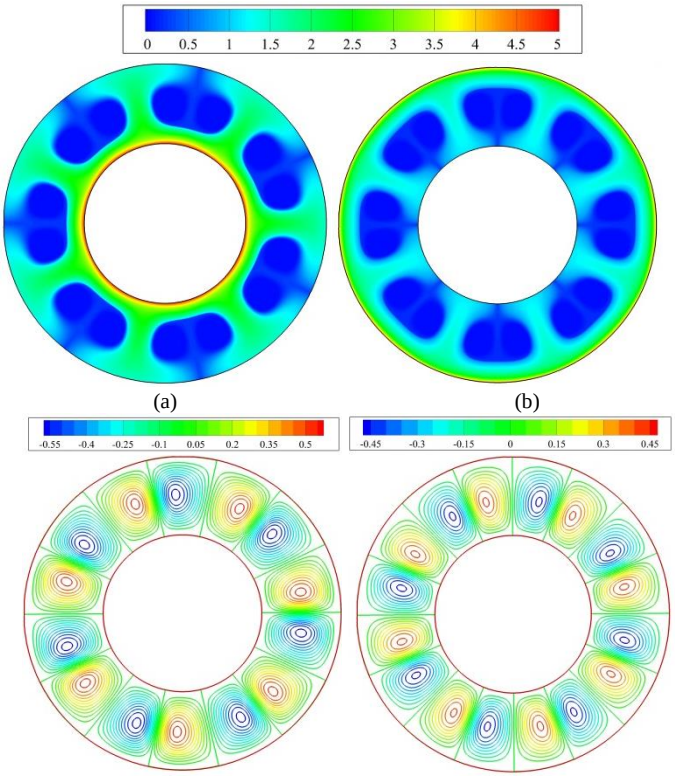

Figure 5. Distributions of charge density (up) and stream function (bottom) for strong injection, C=5, (a) and (c) with inner injection, T=165; (b) and (d) with outer injection, T=255.

2) Irregular flow pattern

For weaker injection strengths ($C < 2$), still taking T close to T_c, we observe that the flow first reaches a quasi-stationary flow pattern. This first process is the same as described in the previous subsection. But after a period of adjustment, the flow destabilizes and bifurcates to another pattern which may be steady or unsteady depending on the injection strength and the value of T. The secondary bifurcation is due to the nonlinear effect because of the high driving parameter.

In Figure 6 we have provided two representative examples of C=1.0 and 0.5. Figure 7 plots the charge density distribution for four cases (points A, B, C and D marked in Figure 6a) to show the flow structure. Figure 6a shows that for C=1.0 and T=600, the inner injection induced flow transits from 7 void regions (Figure 7a) to a stationary state with 8 void regions (Figure 7b); the flow pattern of outer injection transits from 7 void regions (Figure 7c) to a unsteady state with the number of void region periodically changing between 8 and 11. In Figure 7d we can roughly identify 10 void regions.

The phenomenological modal analysis has been performed to understand the evolution of different modes. For C=1.0 and T=600, we have observed in the inner injection case the dominant mode changes from m=7 at point A to m=8 at point B, and in the outer injection case the modes of m=6~12 are excited to a certain amplitude while other modes are very small.

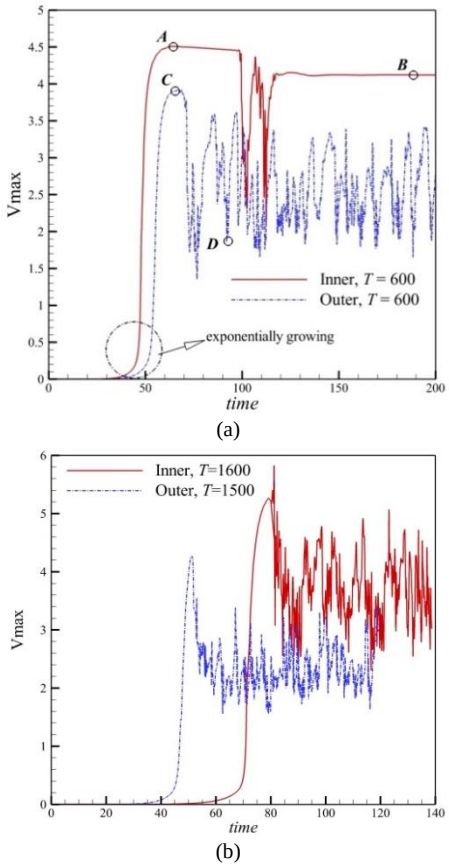

Figure 6. Time histories of the maximum velocity norm for (a) C=1.0 and (b) C=0.5. Note that the values of T_c for C=0.5 are 1444.16 (inner) and 1258.53 (outer), and for C=1.0 are 511.85 (inner) and 513.27 (inner).

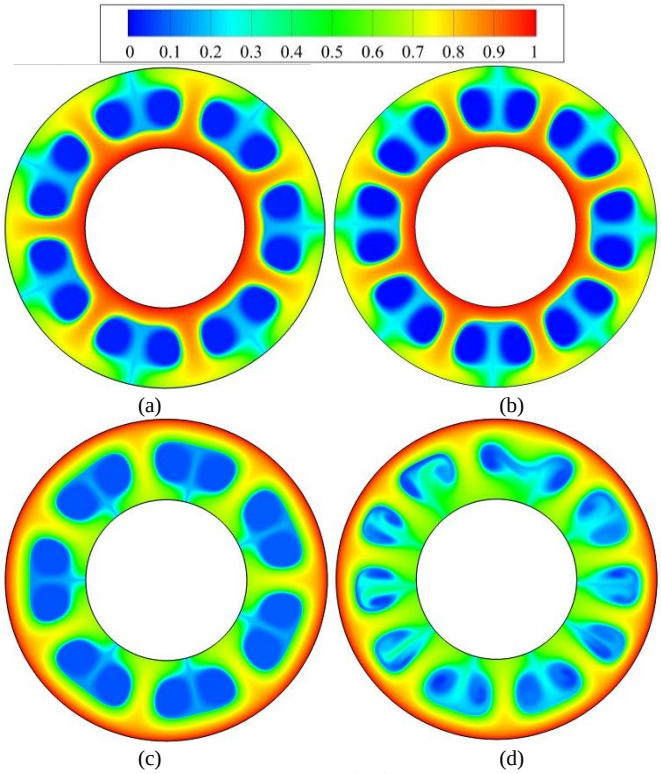

Figure 7. Distributions of charge density for four cases marked in Figure 6a: (a) Point A, (b) Point B, (c) Point C, (d) Point D.

3) Chaotic flow pattern

For very weak injection ($C \leq 0.4$), we observe a chaotic flow pattern. Figure 8 plots the time evolution of Vmax for the representative case of C=0.1. The electric Rayleigh number T is set to 3.0×10^4 and 2.5×10^4 for inner and outer injection, respectively. At the third stage the velocity signals show dramatic fluctuations around an average value.

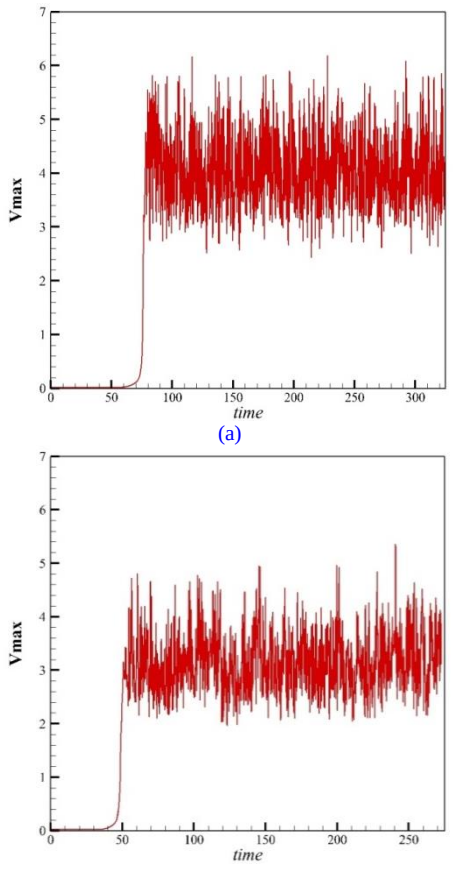

Figure 8 Time histories of the maximum velocity norm for weak injection regime, C=0.1, (a) inner injection, T=3×10^4, and (b) outer injection, T 2.5×10^4. Note that the values of T_c for inner and outer injection are 26470.11 and 20827.23, respectively.

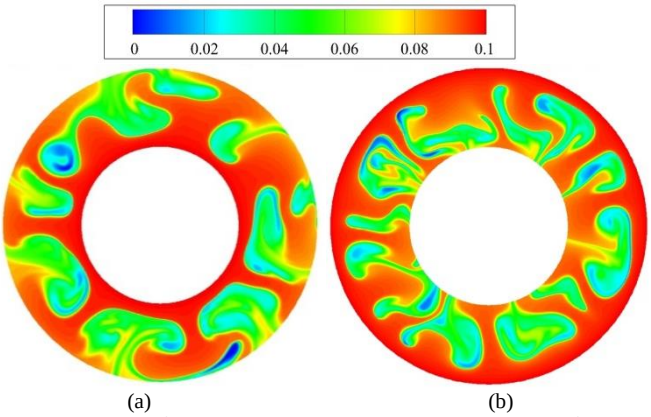

Figure 9 Snapshots of charge density distribution at the chaotic state for weak injection, C=0.1, (a) inner, 3×10^4; (b) outer, T = 2.5×10^4.

Two snapshots of the charge density distribution are depicted in Figures 9a and 9b, which represent very irregular flow motions. Though we can still roughly distinguish the charge-free region from the charge-covered region, the number, shapes and positions of these charge-free regions are continually changing over the entire time period. When the injection strength is weak, the charge density in the charge-covered region takes the value of C because of the weak Coulomb repulsion between charges [38].

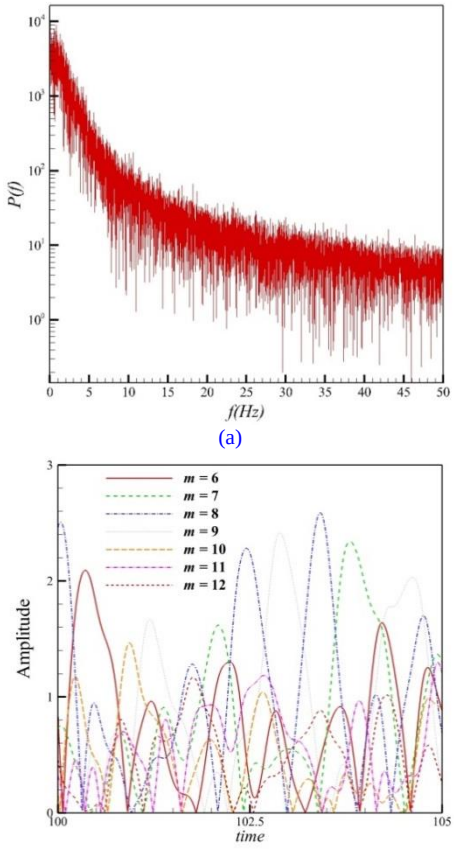

Figure 10 (a) Semilog plots of the pwer spectral curves corresponding to Vmax versus *time* plotted in Figure 8a and (b) a slice of the time evolution of the modal amplitudes, inner injection, C=0.1, T=3×10^4.

The spectral analysis with the volatile signals of velocity shows a broadband spectrum with an exponential decay (see Figure 10a), which reveals the chaotic nature of the flow motions. By checking the time evolution of the modal components (Figure 10b), all modes (m = 1 ~ 15) are excited. The interaction between these excited modes leads to the chaotic flow pattern. In Figure 10b, only the modes of m = 7 ~ 12 are plotted to simplify the display.

4.4 DISCUSSION

A characteristic feature of Coulomb-driven convection with the symmetrical electrode geometry lies in its subcritical nature of the linear bifurcation. For a full description of the subcritical bifurcation, please refer to [2] or [3]. Here we highlight that this type of bifurcation is based on the fact that a stable electroconvective motion requires the maximum fluid velocity to be higher than the ionic velocity [39, 40]. Once the system losses its linear stability, the liquid velocity will increase in time until this condition is satisfied. Since the velocity of the liquid that returns towards the injector is

greater than the drift velocity of the emitted ions, there is a region where the ions cannot enter, and this region appears void of charge, as we showed in the previous subsection. We have compared the fluid velocity and the electric field at the third stage for each test case, and have found that this condition is always fulfilled. Since the subcritical nature of the bifurcation leads to a finite amplitude electroconvection, the convective flow may not always be viscous dominated, even in the neighborhood of the linear stability criterion

Once the electroconvective motion is fully developed, its pattern is mainly decided by the electric Reynolds number defined as $R = T/M^2$ [8, 22]. For strong injection, T_c is small and its corresponding value of R is also small, which implies that the viscous effect is dominating, and thus a steady flow pattern is expected. On the contrary, for weak injection, T_c is so high that the corresponding R value is much greater than the transition value (a reference value is 10 [8]) that separates the viscous and inertial dominated regimes. For this case, the inertial effects are dominant, and the system passes from the rest state directly to chaos. The periodic and chaotic flows shown in [16] with a fixed strong injection strength are achieved by increasing T, which essentially equals to the increase of R.

5 CONCLUSIONS

We studied the two-dimensional annular electroconvection induced by unipolar injection in a dielectric liquid lying between two concentric cylinder electrodes. The representative case with the radius ratio between the two concentric circular cylinders of 0.5 was considered. The injection can be either from the inner or outer electrode. This paper extended our recent study with the strong injection [20] to arbitrary strengths. Due to the uniform injection and the highly symmetrical electrode geometry, the problem possesses a hydrostatic solution. The linear stability criterion that corresponds to the onset of flow motion was determined from the direct numerical results and by the linear stability analysis. A good agreement between the results obtained with the two approaches was always obtained. Once the flow enters into the finite amplitude regime and fully develops, we observed that the flow pattern was highly dependent on the injection strength C. For $C \geq 2$, the flow is characterized by a steady convection. For weaker injection strength ($C<2$), a secondary bifurcation arises because of the nonlinear effects. For very weak injection ($C \leq 0.4$), a chaotic flow pattern is observed. These complex flow patterns can be understood by evaluating the relatively important role played by the viscous and inertial effects.

Our present finding with the relationship between the flow pattern and injection strength provides an indirect way to roughly judge the injection regime. In experiments, it is often difficult to know in advance the injection strength. By observing the flow pattern at the critical voltage, we may know the injection strength is strong, weak or extremely weak. In a future work, we will determine the route to chaos for annular electroconvection by continually varying the driving electric Rayleigh number or the dimensionless mobility number, which can be achieved experimentally by adjusting the applied voltage or changing the working liquid, respectively.

ACKNOWLEDGMENT

This work was partially funded by the French Government program “Investissements d’Avenir” (LABEX INTERACTIFS, reference ANR-11-LABX-0017-01) (to Jian Wu), a grant of the French district Poitou- Charentes (to P. Traoré), and partially by financial support from the Spanish Ministerio de Cienciay Tecnología (MCYT) under Research Project No. FIS2011-25161 and Junta de Andalucía under research projects P10-FQM-5735 and P09-FQM-4584 (to A. T. Pérez).

REFERENCES

[1] A. Castellanos, “Electrohydrodynamics,” Springer, New York, 1998.
[2] A. Castellanos, “Coulomb-driven convection in Electrohydrodynamics,” IEEE Trans. Electr. Ins. vol. 26, pp. 1201-1215, 1991.
[3] P. Atten, “Electrohydrodynamic instability and motion induced by injected space charge in insulating liquids,” IEEE Trans. Electr. Ins. vol. 3, pp. 1-17, 1996.
[4] A. Denat, B. Gosse, and J. P. Gosse, “Ion injections in hydrocarbons,” J. Electrostatics, vol.7, pp. 205-225, 1979.
[5] A. Alj, A. Denat, J. P. Gosse, et al., “Creation of charge carriers in nonpolar liquids,” IEEE Trans. Electr. Ins. Vol.2, pp.221-231, 1985.
[6] L. Onsager, “Deviations from Ohm's law in weak electrolytes,” J. Chem. Phys, vol. 2(9), pp. 599-615, 1934.
[7] F. Pontiga and A. Castellanos, “Physical mechanisms of instability in a liquid layer subjected to an electric field and a thermal gradient,” Phys. Fluids, vol. 6.5, pp. 1684-1701, 1994.
[8] P. Atten and L. Elouadie, “EHD convection in a dielectric liquid subjected to unipolar injection: coaxial wire/cylinder geometry,” J. Electrostatics, vol. 34, pp. 279-297, 1995.
[9] Y. K. Suh, “Modeling and simulation of ion transport in dielectric liquids-Fundamentals and review,” IEEE Trans. Dielect. Electr. Ins. vol. 19(3): 831-848, 2012.
[10] F. W. Langford, and D. D Rusu, “Pattern formation in annular convection,” Physica A, vol. 261(1), pp.188-203, 1998.
[11] J. Fernández and R.. Poulter, “Radial mass flow in electro-hydrodynamically-enhanced forced heat transfer in tubes,” Int. J. Heat Mass Transfer, vol. 30, pp. 2125-2136, 1987.
[12] A. T. Richardson and R. Poulter, “Electrophoretic instability in a diffusion-free dielectric liquid in an annular geometry,” J. Phys. D: Appl. Phys. vol. 9, pp. L45, 1976.
[13] A. T. Richardson, “The linear instability of a dielectric liquid contained in a cylindrical annulus and subjected to unipolar charge injection,” Q. J. Mech. Appl. Math. vol. 33, pp. 277-292, 1980.
[14] N. Agrät and A. Castellanos, “Linear convective patterns in cylindrical geometry for unipolar injection,” Phys. Fluids, vol. 2, pp. 37-44, 1990.
[15] D. V. Fernandes, H. D. Lee, S. Park, and Y. K. Suh, “Electrohydrodynamic instability of dielectric liquid between concentric circular cylinders subjected to unipolar charge injection,” J. Mech. Sci. Tech. vol. 27, pp. 461-467, 2013.
[16] D. V. Fernandes, H. D. Lee, S. Park, and Y. K. Suh, “Numerical simulation of the electro-convective onset and complex flows of dielectric liquid in an annulus,” J. Mech. Sci. Tech. vol. 26, pp. 3785-3793, 2012.
[17] P. Traoré and A. T. Pérez, “Two-dimensional numerical analysis of electroconvection in a dielectric liquid subjected to strong unipolar injection,” Phys. Fluid, vol. 24, pp. 037102, 2012.
[18] P. Traoré and J Wu, “On the limitation of imposed velocity field strategy for Coulomb-driven electroconvection flow simulations”, J. Fluid Mech., vol. 727, R3, 2013.
[19] J. Wu, P. Traoré, and C. Louste, “An efficient finite volume method for electric field–space charge coupled problems,” J. Electrostatics, vol. 71(3), pp. 319-325, 2013.

[20] J. Wu, P. A. Vázquez, P. Traoré, and A. T. Alberto, "Finite amplitude electroconvection induced by strong unipolar injection between two coaxial cylinders," Phys. Fluid, Vol. 26, pp. 124105, 2014.
[21] R. Tobazéon, "Electrohydrodynamic instabilities and electroconvection in the transient and AC regime of unipolar injection in insulating liquids: A review," J. Electrostatics, vol. 15(3), pp. 359-384, 1984.
[22] J. C. Lacroix, P. Atten, and E. J. Hopfinger, "Electroconvection in a dielectric layer subjected to unipolar injection," J. Fluid Mech., vol. 69, pp. 539-563, 1975.
[23] B. Malraison and P. Atten, "Chaotic behavior of instability due to unipolar ion injection in a dielectric liquid," Phys. Rev. Lett., vol. 49, pp. 723-726, 1982.
[24] A. Denat, B. Gosse and J. P. Gosse, "Ion injections in hydrocarbons", J. Electrostatics, vol. 7, pp. 205-225, 1979.
[25] F. M. J. McCluskey, P. Atten, and A. T. Pérez, "Heat transfer enhancement by electroconvection resulting from an injected space charge between parallel plates," Int. J. Heat Mass Transfer, vol. 34(9), pp. 2237-2250, 1991.
[26] X. Zhang, "Electro-optic signatures of turbulent electroconvection in dielectric liquids", Appl. Phys. Lett., vol. 104(20), pp. 202901, 2014.
[27] J. H. Ferziger and M. Perić, "Computational methods for fluid dynamics," Berlin: Springer, 2002.
[28] P. Traoré, Y. M. Ahipo, and C. Louste, "A robust and efficient finite volume scheme for the discretization of diffusive flux on extremely skewed meshes in complex geometries," J. Comput. Phys. vol. 228, pp. 5148-5159, 2009.
[29] S. V. Patankar and D. B. Spalding, "A calculation procedure for heat, mass and momentum transfer in three-dimensional parabolic flows," Int. J. Heat Mass Transfer, vol. 15, pp. 1787-1806, 1972.
[30] C. M. Rhie and W. L. Chow, "Numerical study of the turbulent flow past an airfoil with trailing edge separation," AIAA J. vol. 21(11), pp. 1525-1532, 1983.
[31] P. H. Gaskell and A. K. C. Lau, "Curvature-compensated convective transport: SMART, A new boundedness-preserving transport algorithm," Int. J. Numer. Meth. Fluids, vol. 8, pp. 617-641, 1988.
[32] D.J. Mavriplis, "Revisiting the least-squares procedure for gradient reconstruction on unstructured meshes," AIAA Paper, 2003-3986, 2003.
[33] J. Wu, and P. Traoré, "A finite volume method for electro-thermo-convective phenomena in a plane layer of dielectric liquid," Numer. Heat Transfer A-Appl., DOI:10.1080/10407782.2014.986410, accepted for publication.
[34] P. Atten, F. M. J. McCluskey, and A. T. Pérez, "Electroconvection and its effect on heat transfer," IEEE Trans. Electr. Ins., vol. 23(4), pp. 659-667, 1988.
[35] P. Atten, and R. Moreau, "Stabilité électrohydrodynamique des liquides isolants soumis à une injection unipolaire," J. Mécanique vol. 11(3), pp. 471-521, 1972.
[36] P. Atten, and J. C. Lacroix, "Non-linear hydrodynamic stability of liquids subjected to unipolar injection," J. Mécanique vol. 18, pp. 469-510, 1979.
[37] P. Tsai, Z. A. Daya, V. B. Deyirmenjian, et al. "Direct numerical simulation of supercritical annular electroconvection," Phys. Rev. E, vol. 76(2), pp. 026305, 2007.
[38] A. Castellanos, and P. Atten, "Numerical modeling of finite amplitude convection of liquids subjected to unipolar injection," IEEE Trans. Ind. Appl. IA-23, pp. 825-830, 1987.
[39] N. Felici, "Phénomènes hydro et aérodynamiques dans la conduction des diélectriques fluids", Revue Générale de l'Electricité vol. 78, pp. 717-734, 1969.
[40] P. Atten P, and J. C. Lacroix, "Non-linear hydrodynamic stability of liquids subjected to unipolar injection", Journal de Mécanique, vol. 18, pp. 469-510, 1979.

Jian Wu (M'13) was born in Jiangxi, China, in 1985. He received the B.Eng. degree in thermal energy and power engineering, the B.B.A. degree in business administration, and the M.Eng. degree in refrigeration and cryogenic engineering from Harbin Institute of Technology (China) in 2006, 2006, and 2008, respectively. He obtained his Ph.D. degree in fluid mechanics from University of Poitiers, France, in Sept. 2012.

From Oct. 2012 to Oct. 2014, he worked as a Research Engineer at PPRIME Institute, University of Poitiers (France). Currently he is a visiting researcher of University of Seville (Spain). His areas of research include electro-hydrodynamics, electro-thermo-hydrodynamics, and computational fluid dynamics. He has coauthored 17 peer-reviewed journal papers and about 20 conference papers.

Dr. Wu is a member of IEEE Dielectrics and Electrical Insulation Society and IEEE Industry Applications Society, and a member of European Mechanics Society.

Philippe Traoré was born in Grenoble, France in September 1963. He graduated from the Superior National Engineer School of Aeronautical Constructions of Toulouse, France in 1987 and received, from University of Toulouse, the Ph.D. degree in fluid mechanics in 1996.

He is currently the deputy director of the mechanical department of the University of Poitiers (France) where he teaches fluid mechanic and scientific computation. His research interests focus on general Computational Fluid Dynamic, two-phase flows, granular media as well as on Electro-hydrodynamic.

Pedro A. Vázquez was born in Seville, Spain in 1969. He received his B.Sc degree from the University of Seville, Spain in 1992, and the Ph.D. degree in Physics from the same university in 1998. He is currently Associate Professor at the Departement of Applied Physics III of the University of Seville, Spain.

Alberto T. Pérez was born in El Puerto de Santa María Cádiz, (Spain) in 1962. He obtained a Bachelor degree from the University of Seville (Spain) in 1985 and a PhD from the same university in 1989.

He is currently Professor at the University of Seville. He has co-authored more than 40 papers on Electro-hydrodynamics, Cohesive Granular Materials and Suspensions in Dielectric Liquids. He was Invited Professor at the Universities of Poitiers (2007 and 2013) and Nice (2008), both in France, and Invited Researcher at the LPMC-CNRS in Nice (2003). He served as Vice Dean of the Faculty of Physics at the University of Seville for 12 years.

Dr. Pérez is member of the American Physical Society.